Microscopic Structure and Solvation in Dry and Wet Octanol†

Bin Chen‡ and J. Ilja Siepmann*

Department of Chemistry and Department of Chemical Engineering and Materials Science, University of Minnesota, 207 Pleasant Street SE, Minneapolis, Minnesota 55455-0431

Received: August 25, 2005; In Final Form: October 3, 2005

Octanol−water partition coefficients are extraordinarily successful for correlating and predicting numerous processes of pharmacological and environmental importance. The amphiphilic nature of the 1-octanol molecules allows the octanol phase to mimic the complexities of many different environments ranging from biomembranes to soil. However, the structural details of the octanol phase and whether its structure is altered upon water saturation are not yet fully understood. Configurational-bias Monte Carlo simulations in the Gibbs ensemble demonstrate that a diverse spectrum of hydrogen-bonded aggregates exists in dry and wet 1-octanol, and that water saturation substantially alters the 1-octanol environment from predominantly linear aggregates in dry octanol to larger cylindrical micelles with water cores in wet octanol. These simulation results are able to reconcile the conflicting views (chainlike or water-centered aggregates vs spherical micelles) of the 1-octanol structure inferred from thermodynamic arguments, spectroscopic measurements, and diffraction experiments. Calculated partition constants quantify the influence of water saturation on the solubility characteristics of the dry and wet octanol phases.

1. Introduction

The partitioning of a solute between a polar aqueous and a nonpolar organic phase is often the rate-limiting step in biological and environmental processes. The 1-octanol−water partition coefficient, K_{OW}, and the corresponding Gibbs free energy of transfer, $\Delta G_{OW} = -RT \ln K_{OW}$, for a given solute are probably the most important input parameters used in quantitative structure−activity relationships to correlate and predict a plethora of solute properties,[1,2] including the pharmacokinetic characteristics of drug compounds in biophases (membranes, adipose tissue, and body fluids[3−5]) and the toxicity and transport of pollutants in soil/groundwater systems.[6,7]

The success of 1-octanol as a model solvent for a surprisingly diverse range of systems has been generally attributed to its amphiphilic nature (a hydrophilic hydroxyl group coupled to a lipophilic alkyl tail) which leads to a microheterogeneous phase.[8−12] The structures of dry and wet octanol have been investigated by a plethora of experimental techniques[9,13−16] and using thermodynamic arguments[8] or molecular dynamics simulations,[10−12] but a consensus view has not yet emerged on the types of aggregates formed in the octanol phases and on whether water saturation leads to a substantial structural reorganization. From some studies,[8,13,15,16] it was concluded that linear oligomers of the Zachariasen type[17] should be the predominant aggregates in neat octanol, whereas small water-centered aggregates should appear upon addition of water (see Figure 1). In contrast, X-ray diffraction patterns for both dry and wet octanol are remarkably similar[9] from which it was inferred that structural reorganization does not occur. A model using medium-size reverse micelles with spherical shapes (see Figure 1) was found to be consistent with the observed diffraction patterns.[9]

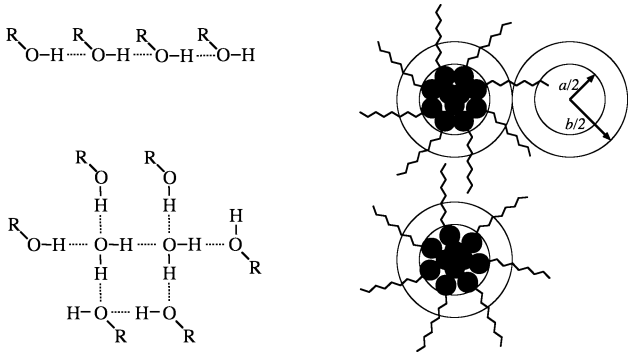

Figure 1. Schematic drawings of models used to explain various experimental results. (Left) Using thermodynamic arguments Marcus[8] suggested that chainlike aggregates are dominant in neat 1-octanol, while small water-centered aggregates are preferred in water-saturated 1-octanol. (Right) From X-ray diffraction experiments Franks et al.[9] conjectured structures dominated by spherical micelles for both dry and wet octanol, but differing in maximum aggregation number (12 and 16), size of the polar core (a = 8.8 and 10.0 Å), and distance of closest approach (b = 14.4 and 17.1 Å).

In addition to the uncertainty of the microscopic structure of the octanol phase, the effect of water on the solvent characteristics of wet octanol and the magnitude of the (fictitious) $\Delta G_{O\rightarrow O^*}$ of a solute between dry and wet 1-octanol are controversial.[1,18−20]

The purpose of this paper is to provide new information on the structure and solvation in dry and wet 1-octanol which can reconcile the conflicting observations mentioned above. Previously, we reported the results of a simulation study of octanol−water partitioning[21] using the OPLS (optimized parameters for liquid simulation) force field.[22−24] Although these earlier simulations provided a wealth of information on the qualitative differences for solvation in dry and wet 1-octanol,[21] a quantitative comparison with experiments could not be made because the saturation concentration of water in 1-octanol was found to be about a factor of 3 too low for the OPLS model.

† Part of the special issue "Michael L. Klein Festschrift".

* Corresponding author: siepmann@chem.umn.edu.

‡ Present address: Department of Chemistry, Louisiana State University, Choppin Hall, Baton Rouge, LA 70803-1804.

10.1021/jp0548164 CCC: $33.50
Published on Web 11/16/2005

2. Simulation Methods

Configurational-bias Monte Carlo (CBMC) simulations[25,26] in the Gibbs ensemble (GE)[27] are ideally suited for an investigation of the octanol−water partitioning system because these simulations employ two or three separate simulation boxes which are in thermodynamic contact (analogous to the experimental setup). As a result, the properties of the coexisting phases (e.g., structures, mutual solubilities, and solute partitioning) can be determined directly from a single simulation.[21,28−30] Two different systems were used here to investigate the effect of water on the solvent characteristic and structural organization of the dry and wet 1-octanol phases: system G/O (vapor/dry 1-octanol) and system G/O*/W (vapor/wet 1-octanol/water). In addition to 1-octanol and water solvent molecules, the simulated systems also contained eight types of solute molecules: methane to *n*-butane and methanol to 1-butanol. System G/O consisted of 580 methane (mainly in the vapor phase), 50 ethane, 10 propane, 2 *n*-butane, 1 methanol, 1 ethanol, 1 1-propanol, 1 1-butanol, and 240 1-octanol molecules. In addition, system G/O*/W contained 864 water molecules. With the exception of 1-octanol (for which the saturated vapor pressure and aqueous solubility are exceedingly low[1]), all molecule types were allowed to swap between phases.

Initially, all solute molecules were placed in the gas phase and the second and third (only for system G/O*/W) simulation boxes contained neat liquid phases. The equilibration process started with a canonical trajectory of the solvent box(es), followed by an isobaric−isothermal trajectory of the solvent box(es). Once preequilibration was achieved for the neat solvent phase(s) as monitored by converged potential energy and specific density, the Gibbs ensemble equilibration was started which in addition to the regular molecular translations, molecular rotations, and CBMC conformational changes[25,26] for articulated molecules (sampling the bond angle bending and torsional degrees of freedom) and volume exchanges with the pressure bath, allows for CBMC swaps of entire solute and water molecules and for CBMC identity swaps[31,32] between the phases. In the latter move, a molecule is converted to a larger molecule (say, water to methanol) in one phase and the reverse conversion (methanol to water) occurs in another phase, thereby equilibrating the chemical potential difference between the two species.

Using the Gibbs ensemble approach, the Gibbs free energy for the transfer of a solute from the gas to liquid phase can be calculated directly from the number density ratio[32−35]

$$\Delta G_{\text{trans}} = -RT \ln K_{\text{trans}} = -RT \ln\left(\frac{\langle \rho_{\text{liquid}} \rangle}{\langle \rho_{\text{gas}} \rangle}\right)_{\text{eq}} \qquad (1)$$

where $\langle \rho_{\text{liquid}} \rangle$ and $\langle \rho_{\text{gas}} \rangle$ are the ensemble-averaged solute number densities (which are mechanical properties given in units of molecules per unit volume, Å^3, or moles per 10^{-3} m^3) for the liquid and gas phases, respectively, at equilibrium. The variables R and T are the molar gas constant and absolute temperature. If a given solute is found to partition very strongly into a specific phase (for example, the Gibbs free energy of transfer from G to O* for 1-butanol is about −24 kJ/mol corresponding to a partition constant of about 16000, see section 4), then statistical problems can arise for the computation of the solute number density in the other phase. To some extent, this can be overcome by adjusting the phase ratio as done also in experimental work. However, solely adjusting the phase ratio is not sufficient for a situation with multiple solutes that have free energies of transfer differing over a wide range (e.g., methane vs 1-butanol). To improve the statistical precision, additional "balancing factors" were used to reduce the probability that the otherwise highly soluble alcohol solutes are found in the 1-octanol phase. These balancing factors are pre-set external potentials acting on a specific molecule in a specific phase which are very similar in spirit to the η parameter in expanded-ensemble simulations[36] and can be removed in the calculation of the Gibbs free energies of transfer.[37] The following η/k_B values were used for methanol, ethanol, 1-propanol, and 1-butanol in the 1-octanol phase: 50, 325, 600, and 900 K, respectively. With the phase ratio and the balancing factors selected here, the total numbers of solute molecules in the octanol and water phases are typically less than two, and these low solute concentrations should not significantly alter the properties of these solvent phases.

Four independent simulations were carried out for each of the two systems (G/O and G/O*/W). Equilibration of the GEMC trajectories was monitored by following the potential energies, specific densities, and compositions of the phases. The production periods for each independent GEMC simulation consisted of more than 10^5 Monte Carlo cycles (where one cycle consists of N_{sys} moves with N_{sys} being the total number of molecules, i.e., 886 and 1750 molecules for systems G/O and G/O*/W, respectively).

The interactions of water and of the alkanes/alcohols were described by the rigid TIP4P model[38] and the transferable potentials for phase equilibria united-atom (TraPPE-UA) force fields.[26,39,40] The articulated alkane and alcohol molecules were treated as semiflexible chains with fixed bond length but flexible bond angle bending and torsional degrees of freedom. Spherical potential truncations at 14 Å and analytical tail corrections were employed for the Lennard-Jones interactions.[41] In addition, an Ewald sum with tin-foil boundary conditions was used to compute the electrostatic interactions.[41] The thermodynamic constraints for the simulations were a temperature of 298 K and a pressure of 1 atm.

3. Structural Analysis of the Dry and Wet Octanol Phases

A. Composition. The saturation concentration of water-saturated 1-octanol determined from the simulations using the TIP4P/TraPPE-UA force fields is $x_W(O^*) = 0.21 \pm 0.04$, i.e., slightly lower than the recommended experimental value of 0.27 but within the range of experimental data ($0.20 < x_W(O^*) < 0.29$).[1] The ratio of 0.21/0.27 between the predicted and the recommended saturation concentrations corresponds to a free energy error of about 0.6 kJ/mol. However, agreement is much better than for earlier simulations yielding $x_W(O^*) = 0.09$ for the TIP4P/OPLS force fields[21] and $x_W(O^*) = 0.16$ for SPC/modified GROMOS96 force fields.[12]

B. Size and Shape of Hydrogen-Bonded Aggregates. As discussed in the Introduction, hydrogen-bonded aggregates are the most important structural motif present in the neat and water-saturated octanol phases. A hydrogen-bonded aggregate is defined here as a collection of molecules where every molecule shares at least one hydrogen bond with another molecule belonging to the same aggregate. In principle, aggregates could be sorted by aggregation number and architecture (linear, branched, or ring topology; see, for example, refs 42−44), but given the broad size distributions observed here (see below), no further division according to architecture was attempted.

Unfortunately, an unambiguous definition for a hydrogen bond does not exist and there is a continuum from strong to weak hydrogen bonds.[45−48] To show that the qualitative conclusions of this work are independent of the precise nature of the set of criteria used to define a hydrogen bond, we have used

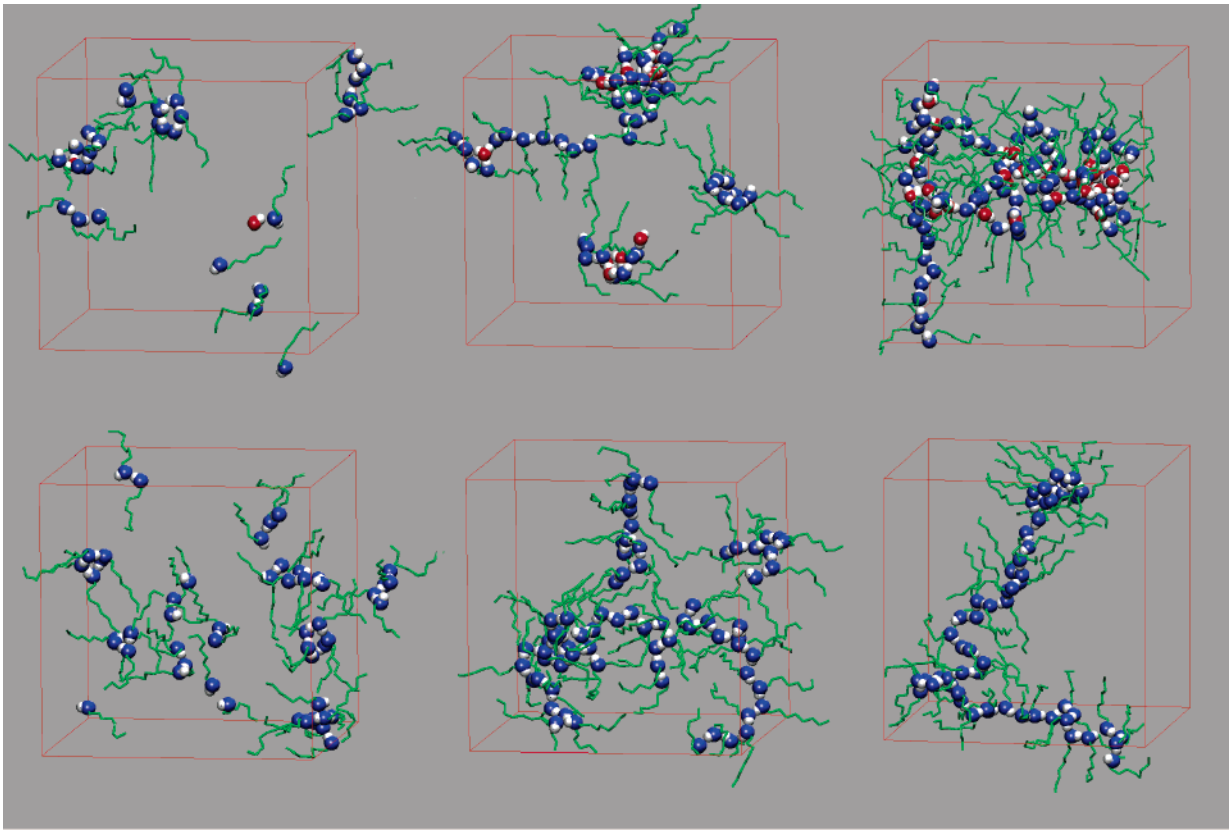

Figure 2. Snapshots of hydrogen-bonded aggregates in water-saturated (top) and neat (bottom) octanol phases. The left, middle, and right columns show aggregates with sizes smaller than 8 molecules, ranging from 9 to 20 molecules, and with more than 60 molecules, respectively. Hydrogen, 1-octanol oxygen, and water oxygen atoms are depicted by white, blue, and red spheres, respectively, whereas a stick representation is used for the alkyl tails. The red cube outlines the periodic simulation cell.

three different criteria as follows: (i) STRICT, $r_{OO} < 3.3$ Å and $r_{OH} < 2.5$ Å and $\cos\theta_{OHO} < -0.4$ and $u_{head} < -13$ kJ/mol; (ii) one based solely on headgroup energy, HE, $u_{head} < -13$ kJ/mol; (iii) one based solely on oxygen−oxygen distance, ROO, $r_{OO} < 3.3$ Å. Here θ_{OHO} is the angle between the bond vector from the donor oxygen to the donor hydrogen and the hydrogen-bond vector from the acceptor oxygen to the donor hydrogen and u_{head} is an intermolecular energy term arising from the Lennard-Jones interactions between oxygen and α-carbon sites and Coulombic interactions between all partial charge sites. Use of the STRICT criteria is more consistent with the observed spatial distributions (see later) and avoids overcounting of pairs that are in close proximity but where the donor hydrogen points away from the acceptor oxygen.[43,44]

From visual inspection of configurations of the dry and wet 1-octanol phases it is immediately evident that both phases contain a very diverse spectrum of hydrogen-bonded aggregates with large variations in size, shape, and architecture. Snapshots of some small, midsized, and large aggregates (selected based on the STRICT criteria) are shown in Figure 2. This diversity of aggregates is not adequately represented in the simple structural models shown in Figure 1, but it is in agreement with the findings of other simulation studies.[10−12]

The distributions of solvent molecules vs the size of hydrogen-bonded aggregates in the octanol phases are shown in Figures 3 and 4. First. it should be noted that although the distributions obtained for the three different hydrogen-bond criteria are not in quantitative agreement (for example, the distributions for the simple ROO criterion are shifted to larger aggregate sizes than those for the restrictive STRICT criteria, with more than 40% of the solvent molecules in wet octanol belonging to clusters with more than 100 molecules for the former criterion and less than 20% for the latter criteria), the overall features are strikingly similar for all three criteria. Thus, in the remainder of this work, we will mainly discuss results that are based on the STRICT criteria and mention explicitly if one of the other criteria is used.

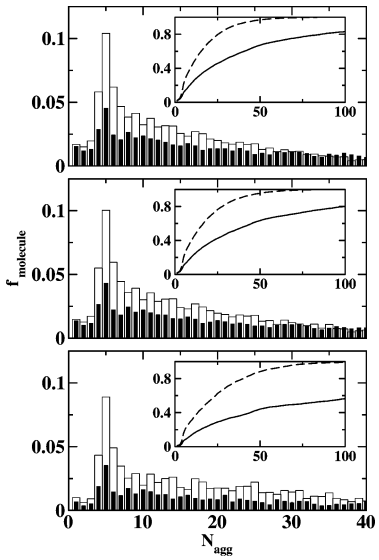

Figure 3. Distributions of solvent molecules (inset, running sum) over hydrogen-bonded clusters with aggregation number N_{agg} found in neat (open histogram and dashed line) and water-saturated (filled histogram and solid line) octanol phases. The top, middle, and bottom parts show the distributions obtained using the STRICT, HE, and ROO criteria for hydrogen bonding.

For both dry and wet octanol, the most important observation is that the distribution over aggregate sizes is essentially flat.

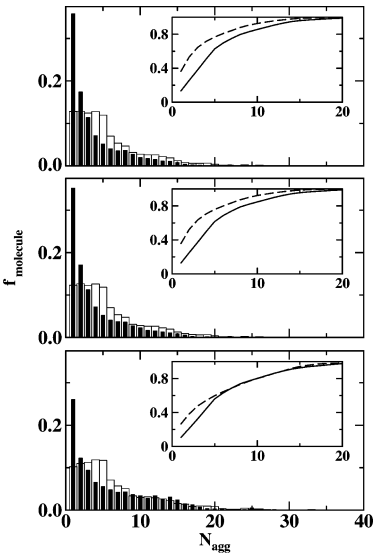

Figure 4. Distributions of molecules over hydrogen-bonded clusters consisting of only octanol molecules (open histogram and solid line) or only water molecules (filled histogram and dashed line) with aggregation number N_{agg} found in the water-saturated octanol phase. The top, middle, and bottom parts show the distributions obtained using the STRICT, HE, and ROO criteria for hydrogen bonding.

A feature that was also observed in the simulation study by MacCallum and Tieleman.[12] There are very few aggregates containing three or fewer molecules, and an aggregation number of 5 appears to be most favorable in both dry and wet octanol. While the "formation of water centered aggregates in which four alcohol molecules are hydrogen-bonded to one water molecule"[13] was predicted for wet octanol from measurements of dielectric constants (see Figure 1), it is observed here that only ≈15% of the pentamers contain one water molecule, whereas more than 80% are made up solely of octanol molecules. Similarly, only 10% of the octamers contain two water molecules, whereas 80% of the octamers contain less water. About 60% of the octanol pentamers in both dry and wet octanol possess a cyclic architecture. In contrast, linear chains appear to be the preferred architecture for the medium-sized aggregates in dry 1-octanol (see Figure 2). Linear chains compete with water-centered micellar aggregates in wet 1-octanol, where the latter contain a substantially higher fraction of water molecules than x_W(O*). Thus, although the structures suggested from thermodynamic and spectroscopic arguments[8,13] (see the left-hand side of Figure 1) are present in the octanol phases, they are definitely not the dominant structural motif.

Franks et al.[9] demonstrated that a simple model (see Figure 1) consisting of spherical micelles with aggregation numbers of 12 and 16 for dry and wet octanol, respectively, can fit the experimental X-ray diffraction pattern very well. The aggregate size distributions obtained from our simulations (see Figure 3) clearly do not support a preference for aggregates of these sizes. Nevertheless, some aggregates with aggregation numbers in the vicinity of 12 and 16 are present in the simulations, and the principal moments of inertia were calculated here for the polar core of these aggregates (see Figure 5). The ratios of the moments of inertia observed for dry (and wet) 1-octanol show a broad distribution ranging from 1.8:1.0:1.0 (1.3:1.0:1.0) to 58:57:1 (28:27:1), i.e., from mildly oblate spheroids to strongly prolate spheroids (or elongated cyclindrical shapes). The median values for the ratios of the moments of inertia are 5.5:4.8:1.0 (3.9:3.4:1.0) showing that cylindrical shapes are strongly favored in both cases, although the aggregates in the wet octanol phase are less elongated. Again, this observation does not depend on the use of a specific hydrogen-bond criterion (see Figure 5). MacCallum and Tieleman found somewhat less elongated shapes for the polar core of the aggregates with ratios of 2.0:1.8:1.0 (1.8:1.6:1.0), but the averaging included all aggregate sizes.[12] Thus, both simulation studies strongly suggest that spherical micelles are not an important structural motif for the dry and wet octanol phases.

One of the most striking observations of this study is the existence of very large hydrogen-bonded aggregates. In fact, about 50% of the water and 1-octanol molecules in wet octanol belong to clusters with aggregation numbers above 25 (see

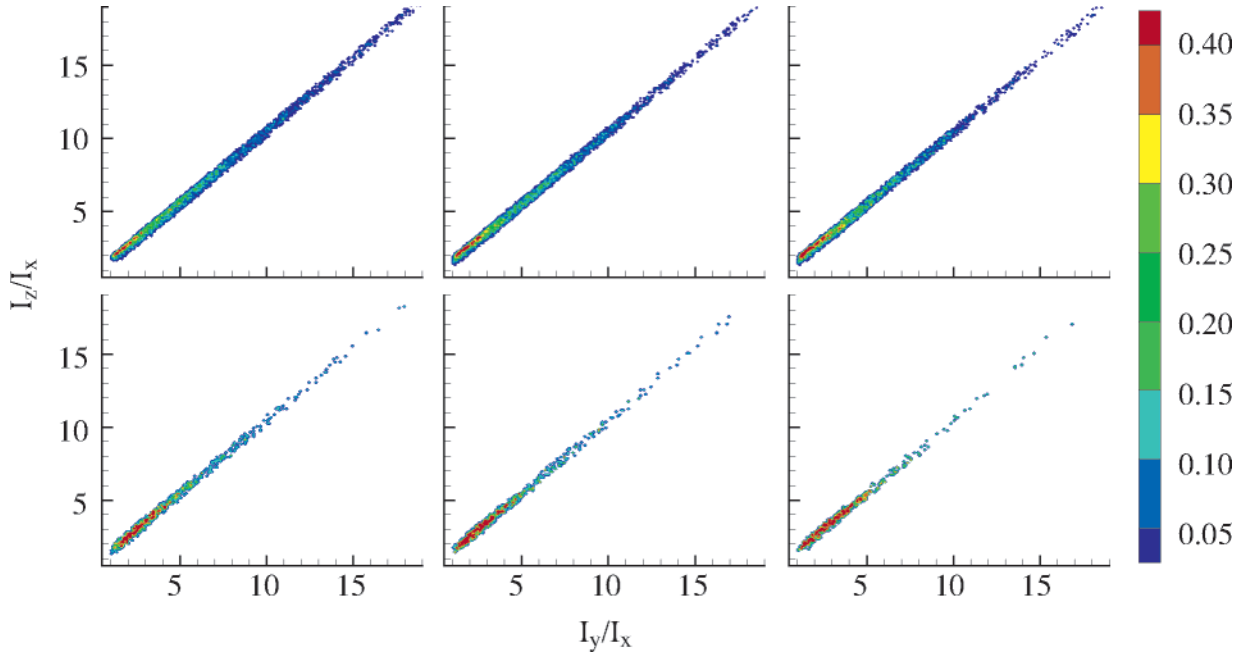

Figure 5. Distributions of the relative moments of inertia for the hydrogen-bonded cores (using only oxygen and polar hydrogen atoms) averaged over (top) all aggregates containing 15 to 17 solvent (water or octanol) molecules in water-saturated octanol (system G/O*/W) and (bottom) containing 11 to 13 octanol molecules in neat octanol (system G/O). The left, middle, and right parts show the distributions obtained using the STRICT, HE, and ROO criteria for hydrogen bonding, respectively.

TABLE 1: Hydrogen-Bond Analysis[49]

	with water		with alcohol[a]	
molecule/phase(system)	donors	acceptors	donors	acceptors
water/W(G/O*/W)	1.94	1.94	0.01	0.01
water/O*(G/O*/W)	0.59	0.59	1.25	0.90
octanol/O*(G/O*/W)	0.23	0.32	0.74	0.74
octanol/O(G/O)		0.98	0.98	

[a] The numbers for hydrogen bonds with alcohols include contributions from 1-octanol and the four alcohol solutes.

Figure 3 (top)). Substantially fewer large clusters were found in dry 1-octanol, and their main structural motif remains long linear chains that are joined at a few branch points (see Figure 2), whereas elongated, water-centered micellar-like aggregates are the dominant component found in wet 1-octanol.

Although the distribution of solvent molecules over aggregate sizes in wet octanol shows a maximum for the pentamer and most of the water molecules are found in larger clusters, it should be pointed out that "isolated"water molecules (without a hydrogen bond to another water molecule) constitute nearly 40% of the water molecules in the wet octanol phase (see Figure 4 (top)) and that less than 10% of the water molecules belong to water droplets consisting of more than 10 molecules. Nevertheless, these water droplets act like a "glue" for the octanol molecules in wet octanol because the aggregate distribution shifts to significantly smaller clusters when only hydrogen-bonding of octanol molecules is considered compared to hydrogen-bonding of all solvent molecules (Figure 4 (top) vs Figure 3 (top)). Furthermore, although there are many water molecules isolated from other water molecules, there are only very few monomeric aggregates when all hydrogen bonds are considered; that is, most of the "isolated" water molecules are involved in hydrogen bonds with up to four surrouding octanol molecules.

C. Local Hydrogen-Bond Analysis. After discussion of the broad distribution over aggregates sizes, we focus attention now on the local hydrogen-bond pattern arising from donor or acceptor interactions in the first solvation shell (see Table 1).[49] The total number of nearest-neighbor contacts for a given water molecule decreases from 3.90 in the aqueous phase to 3.33 in wet octanol (substantially below the value of 4 expected from the idealized aggregates shown in Figure 1). In contrast, the number of hydrogen-bond contacts for octanol increases from 1.96 for dry octanol to 2.03 for wet octanol. The fraction of octanol hydroxyl hydrogens in wet octanol that contribute to a hydrogen bond is very high (0.74 donate to an octanol acceptor and 0.23 to a water acceptor; see Table 1), and the fraction of nondonating octanol hydroxyl groups of about 3% is in good agreement with a value of 3.8% obtained by infrared spectroscopy.[14] The fraction of nondonating octanol hydroxl groups found in dry octanol is about 2%.

In wet octanol, the average number of contacts per molecule of 2.30 ($=3.33 \times 0.21 + 2.03 \times 0.79$, where 0.21 and 0.79 are the saturated molefractions of water and octanol, respectively) is very close to the value of 2.37 predicted for ideal mixing ($=3.90 \times 0.21 + 1.96 \times 0.79$). Thus, water saturation does not result in a significant loss in the total number of hydrogen bonds. Nevertheless, for the wet octanol phase an enhancement of the water concentration is observed for the first solvation shell. The local mole fractions[8] of water surrounding octanol, $x_{W(O)}{}^{L} \approx 0.27$, and water surrounding water, $x_{W(W)}{}^{L} \approx 0.35$, fall substantially above the global water mole fraction of $\approx$0.21. Recent neutron diffraction and empirical potential structure refinement studies of concentrated methanol/water mixture ($x_{MeOH} = 0.7$) carried out by Soper and co-workers[50] provided a similar picture with respect to hydrogen bonding (an exact compensation of the loss of hydrogen bonds per water molecule by the gain of hydrogen bonds per alcohol molecule) and incomplete mixing at the molecular level.

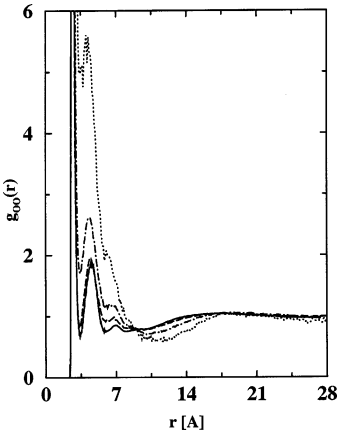

Figure 6. Solvent oxygen−solvent oxygen radial distribution functions. The solid, dashed, dashed−dotted, and dotted lines are used for $g(O_OO_O/O)$, $g(O_OO_O/O^*)$, $g(O_OO_W/O^*)$, and $g(O_WO_W/O^*)$, respectively.

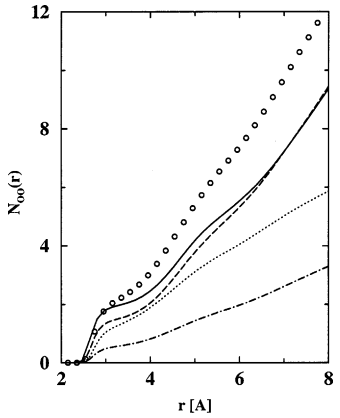

Figure 7. Solvent oxygen−solvent oxygen number integrals. Line styles are as in Figure 6, and $N(O_WO_O/O^*)$ is depicted as circles.

D. Radial and Spatial Distribution Functions. The oxygen−oxygen radial distribution functions (RDFs) and the corresponding number integrals (NIs) for various solvent pairs in the dry and wet octanol phases are shown in Figures 6 and 7. In the following the RDFs and NIs of a specific solvent pair are labeled as $g(A_XB_Y/P)$ and $N(A_XB_Y/P)$, where A and B denote the site with O and M standing for oxygen and (terminal) methyl group, respectively, X and Y denote the molecule type, with O and W standing for octanol and water, respectively, and P denotes the phase with O and O* standing for dry and wet octanol, respectively. There are three different oxygen−oxygen RDFs in the wet octanol phase: $g(O_OO_O/O^*)$, $g(O_OO_W/O^*)$, and $g(O_WO_W/O^*)$. Both $g(O_OO_O/O)$ and $g(O_OO_O/O^*)$ show three sharp peaks $r \approx 2.8$, 4.5, and 7 Å, followed by an extended, shallow depression and a weak but broad fourth peak centered at $r \approx 18$ Å.

The first peak height is largest for $g(O_WO_W/O^*)$ and smallest for $g(O_OO_O/O^*)$. Thus, both O_W and O_O prefer to be surrounded by O_W. In agreement with the enrichment of coordinating water molecules obtained from the hydrogen-bond analysis (see preceding section), the number integrals also support a micro-heterogeneous picture of the wet octanol phase. The simulations yield about twice as many water molecules in the first solvation shell around another water molecule than around the hydroxyl

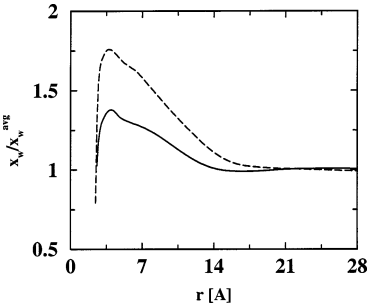

Figure 8. Distance dependence of the ratio of the local mole fraction of O_W surrounding O_O (solid line) and O_W (dashed line) to the average mole fraction of water in the wet octanol phase.

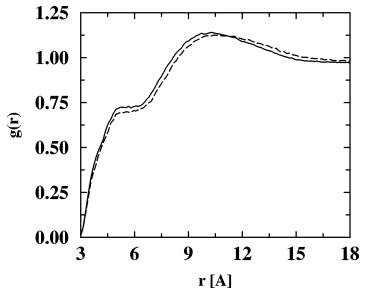

Figure 9. Octanol oxygen−octanol methyl radial distribution functions in the dry (solid line) and wet (dashed line) 1-octanol phases.

group of an octanol molecule (compare the dotted and dashed−dotted lines, respectively, in Figure 7). It is also remarkable that this enrichment persists well beyond the third solvation shell (≈8 Å) where $N(O_WO_W/O^*)$ is still about 70% greater than $N(O_OO_W/O^*)$. Similarly, $N(O_WO_O/O^*)$ falls about 40% above $N(O_OO_O/O^*)$ from the first to the third coordination shell, that is, water molecules are found at the center of the polar regions. This is clearly a reflection of water's ability to form four hydrogen bonds, whereas the alcohols are limited to three. Nevertheless, the first-shell coordination number for water in wet octanol is about 3.8, slightly smaller than in bulk water[47,48] and as would be expected from the idealized eight-membered aggregates shown in Figure 1.

Figure 8 shows the distance dependence of the water enrichment around other polar groups in terms of the local mole fraction enhancement that can be computed from the corresponding number integrals.[40] The mole fraction enhancement around O_O extends to about 15 Å, which is well beyond the three solvation shells discernible in the radial distribution functions. This 15 Å radial enhancement gives an indication of the extension of the largest water droplets in the wet octanol phase. In comparison, the enrichment around O_O extends to about 21 Å, an indication for the separation between water droplets.

Although the oxygen−oxygen RDFs point to a highly structured polar core in both dry and wet octanol, the oxygen-methyl RDFs, $g(O_OM_O/O)$ and $g(O_OM_O/O^*)$, show only a weak peak at $r \approx 10$ Å and a shoulder at $r \approx 5$ Å(see Figure 9). While this shoulder arises from infrequent nearest-neighbor contacts, the weak peak coincides with about half the spacing of the weak fourth peak found for $g(O_OO_O/O)$ and $g(O_OO_O/O^*)$ and appears to be a consequence of a somewhat regular spacing between neighboring aggregates and of the gap between the hydrophilic (oxygen-rich) moieties being occupied by a hydrophobic (methylene and methyl-rich) region.

Calculations of spatial distribution functions (SDFs, see Figure 10) yield further evidence about the limited influence of water saturation on the local structures of the dry and wet 1-octanol phases. The SDFs of the hydroxyl groups show three distinct peaks: (i) $r_{OH} \approx 1.8$ and $\cos\theta_{OHO} \approx -1$ for the hydrogen-bonded peak; (ii) $r_{OH} \approx 2.5$ and $\cos\theta_{OHO} \approx +0.5$ originating from the hydrogen atom that is connected to the acceptor oxygen but not involved in the hydrogen bond; and (iii) $r_{OH} \approx 3.6$ and $\cos\theta_{OHO} \approx -0.75$ arising from a second nearest neighbor. Overall, the SDFs of the hydroxyl groups are quite similar for both octanol phases, but there is slightly more disorder in the wet octanol phase. In contrast, the SDFs for water show significant perturbation of the hydrogen-bond structure found in wet octanol compared to neat water and it appears that the steric hindrance of the octanol tails leads to a strain on the solvated water droplets.

E. Structure Factors. While the microscopic-level structures described above are very rich, they clearly disagree with the structural models inferred from experimental observations (see Figure 1). Thus, it remains to be seen whether the simulated structures can reproduce macroscopic measurements. In the interest of brevity, we will focus on two important aspects, the X-ray diffraction patterns and the Gibbs free energies of transfer between vapor and dry or wet 1-octanol phases (see next section). Figure 11 shows a comparison of the calculated X-ray diffraction intensities for *n*-octane and dry and wet 1-octanol and their experimental counterparts.[9,16] The calculated X-ray diffraction intensities were obtained through Fourier transforms of weighted radial distribution functions using tabulated atomic scattering factors.[51] The overall agreement with experiment for the simulations using the TIP4P/TraPPE combination of force fields is very satisfactory. In particular, it is clearly evident that the broad distribution over diverse aggregates found in the simulations can reproduce both the positions and the relative

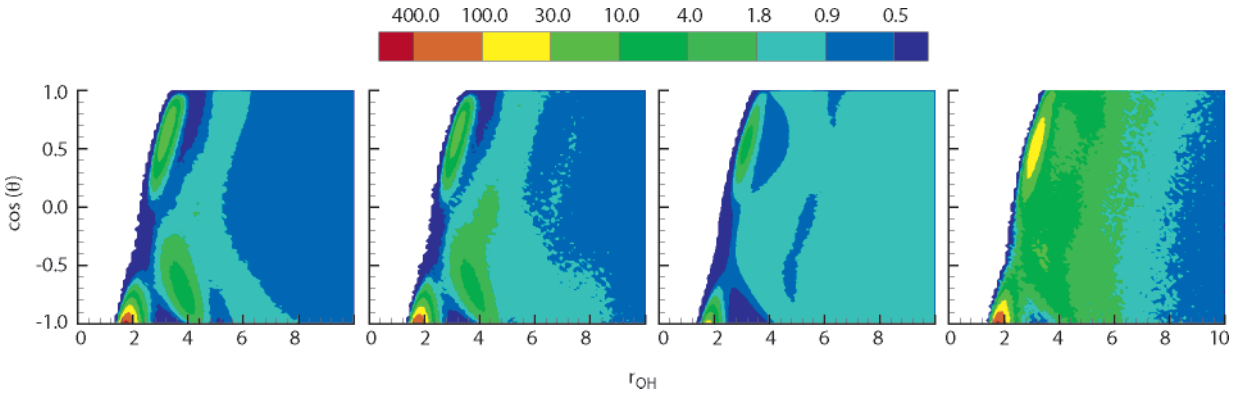

Figure 10. Spatial distributions as functions of the oxygen−hydrogen distance and the hydrogen-bond angle, θ_{OHO} (see discussion of the hydrogen-bond criteria) calculated for octanol in the dry (system (G/O) and wet (system G/O*/W) octanol phases and for water in the water-rich and octanol-rich phases of system G/O*/W (from left to right).

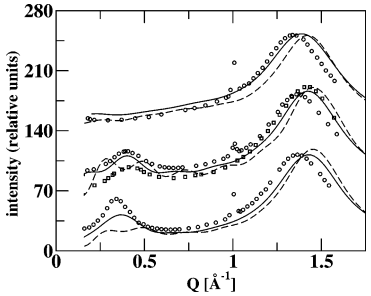

Figure 11. Experimentally measured (circles[9] and squares[16]) and calculated (solid lines for TIP4P/TraPPE (this work) and dashed lines for TIP4P/OPLS[21]) X-ray diffraction intensities for *n*-octane (top, shifted by 140 units), dry octanol (middle, shifted by 70 units), and wet octanol (bottom).

heights of the low-angle diffraction peaks. In dry octanol, the TIP4P/TraPPE simulations give a peak at $Q \approx 0.41$ Å^{-1} compared to peak positions of 0.40 and 0.42 found in two independent experimental studies.[9,16] In wet octanol, the simulated peak is found at 0.37 Å^{-1} and the corresponding experimental peak positions is 0.35 Å^{-1}.[9] This minor difference might be a reflection of the calculated x_W(O*) being about 20% below the experimental saturation limit.

It should also be mentioned here that the diffraction patterns obtained from our earlier simulations using the TIP4P/OPLS force fields[21] deviate significantly from the experimental data. These simulations were shorter and fewer configurations were available for the analysis resulting in more noise. The deviations for the TIP4P/OPLS simulations arise from two factors: an overprediction of the density in the alkyl group region[39] and a substantial underestimation of the solubility of water in octanol, x_W(O*) (as discussed above).

F. Organized Hydrophilic Columns. As discussed in the preceding sections, the RDFs and moment-of-inertia distributions point to long-range ordering of cylindrical aggregates as the source of the low angle diffraction peaks. Instead of describing the overall structure in cartoon format, a snapshot of the wet octanol phase (showing all molecules in the central simulation box and some of the surrounding periodic images) is presented in Figure 12. The main structural motif appears to

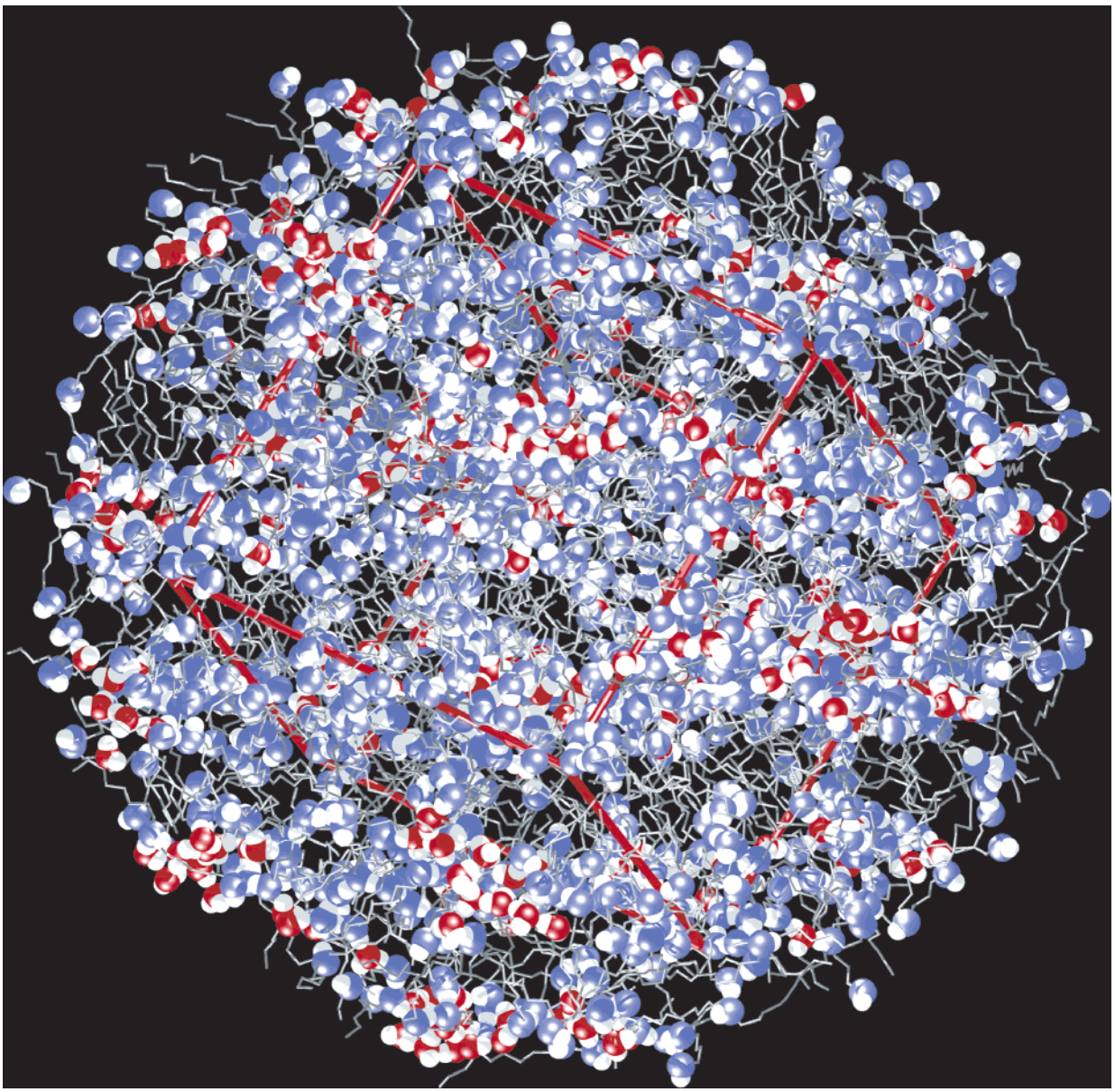

Figure 12. Snapshot of the hydrophilic columns found in wet octanol (system G/O*/W). Color scheme as in Figure 2. The red cube outlines the periodic simulation cell and, for clarity, a few molecules from the surrounding periodic images are also shown.

TABLE 2: Gibbs Free Energies of Transfer in Units of kJ/mol[a]

	simulation		experiment[1,19,52]	
solute	G → O	G → O*	G → O	G → O*
methane	$+1.83_6$	$+1.93_6$		+2.14
ethane	-2.25_8	-2.12_9		−2.68
propane	-4.92_{10}	-4.78_{10}		−5.27
n-butane	-7.63_{10}	-7.43_{10}		−7.78
methanol	-16.3_7	-17.3_3	−16.17	−17.14
ethanol	-18.3_7	-19.1_4	−18.22	-19.15
1-propanol	-20.8_6	-21.7_3	−20.98	-21.81
1-butanol	-23.4_7	-24.3_3	−23.88	−24.64

[a] The subscripts denote the error of the mean calculated from the four independent simulations for each system.

be long hydrophilic columns that are ordered on a larger length scale, i.e., the long axes of the columns are parallel and the spacing between columns is somewhat regular (see Figures 6 and 11). However, the water-rich columns are interconnected through chainlike extensions consisting predominantly of octanol molecules. These water-centered columns might possess somewhat smaller dipole moments, thereby explaining the decrease in dielectric constant upon addition of water.[13,15] A similar structural motif was also observed in earlier simulations by Debolt and Kollman,[10] but it is different from the randomly oriented prolate aggregates found by MacCallum and Tieleman.[12]

4. Solvation in Dry and Water-saturated Octanol Phases

A. Gibbs Free Energies of Transfer. The $\Delta G_{G\rightarrow O}$ and $\Delta G_{G\rightarrow O^*}$ values for *n*-alkanes and primary alcohols calculated for the TIP4P/TraPPE force fields are in excellent agreement with the experimental data (mean unsigned error of less than 0.3 kJ/mol; see Table 2). In particular, it is noteworthy that the agreement extends to the (fictitious) transfer between dry and wet octanol phases. In contrast, the earlier calculations for the TIP4P/OPLS force fields resulted in a larger mean unsigned error of 1.5 kJ/mol. The agreement for both of these studies is actually rather good considering that Best et al. reported a mean unsigned error of 5.6 kJ/mol for the relative free energies, $\Delta\Delta G_{G\rightarrow O^*}$, of some solute conversions in water-saturated octanol.[11]

The calculated $\Delta G_{O\rightarrow O^*}$ values for all alcohol solutes are negative by ≈1.0 kJ/mol (the corresponding experimental value reported by Dallas and Carr[19] is 0.9 kJ/mol), i.e., the wet octanol phase with its water-centered aggregates is a more favorable solvent for them. In contrast, the *n*-alkane solutes exhibit positive $\Delta G_{O\rightarrow O^*}$ ranging from 0.1 to 0.2 kJ/mol for methane to *n*-butane. Experimental data for short alkanes are not available but a $\Delta G_{O\rightarrow O^*}$ of 0.25 kJ/mol for *n*-nonane was determined by Dallas and Carr.[19] Values of similar magnitude for *n*-alkanes and 1-butanol were obtained by Schantz and Matire,[18] but Bernazzani et al.[20] measured much larger values of −1.8 kJ/mol for 1-butanol and from 2.0 to 1.3 kJ/mol for *n*-hexane to *n*-octane.

B. Solvation Structure. To analyze the effect of water saturation on solubilities, RDFs and NIs for solute−solvent pairs were calculated. The solute oxygen−solvent oxygen NIs for both methanol and 1-butanol demonstrate that the hydroxyl groups of the alcohol solutes are embedded in the polar regions of the dry and wet octanol phases (see Figure 13). The average oxygen coordination numbers for the methanol and 1-butanol hydroxyl oxygens (using a cutoff distance of 3.5 Å) are 2.1 and 2.0 for the dry 1-octanol phase, respectively, while these numbers (summed over O_O and O_W) increase by about 0.3 for both solutes in the wet 1-octanol phase. In contrast, when the second solvent shell is included (out to 6.0 Å) an increase of 2.6 is found for the methanol hydroxyl oxygen (from 5.8 in the dry octanol phase to 8.4 in the wet octanol phase), which is noticeably larger than the increase of 1.7 for 1-butanol (from 5.4 to 7.1).

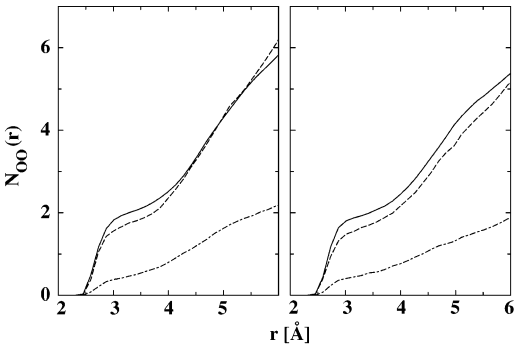

Figure 13. Solute oxygen−solvent oxygen number integrals for methanol (left) and 1-butanol (right). The solid, dashed, and dashed−dotted lines denotes $N(O_{solute}O_O/O)$, $N(O_{solute}O_O/O^*)$, and $N(O_{solute}O_W/O^*)$, respectively.

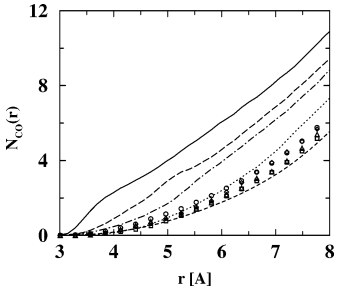

Figure 14. Solute methyl-solvent oxygen (summed over O_O and O_W) number integrals in the wet octanol phase. The following symbols and line styles are used to denote the solute type: methane (circles), ethane (squares), propane (diamonds), *n*-butane (upper triangles), methanol (solid line), ethanol (long dashed line), 1-propanol (dashed−dotted line), and 1-butanol (dotted line). For comparison the corresponding NI for 1-octanol is shown as dashed line.

The solute methyl-solvent oxygen NIs in the wet octanol phase are plotted in Figure 14. The oxygen coordination number around the methyl group of the alcohol solutes decreases significantly with increasing chain length (and a similar change is observed for the dry octanol phase). For example, the first-shell oxygen coordination numbers (up to a distance of 4.5 Å) are 3.9 and 0.5 around the methyl groups of methanol and 1-butanol solutes, respectively. The coordination shell of the 1-butanol methyl group is quite similar to that found for the alkane solutes for which the NIs do not show a strong dependence on the alkane length.

These observations support that methanol preferentially partitions into the core of the water-rich aggregates, while 1-butanol is found at the interface of these aggregates, thereby explaining the decreasing magnitude of the negative $\Delta G_{O\rightarrow O^*}$ values with increasing length of the alcohol solutes seen in the experimental[19] and simulation data (see Table 2). Thus, the more favorable solvation of the alcohol solutes in wet octanol appears to be driven by a more favorable enthalpy arising from a better hydrogen-bond environment.

The relatively small number of oxygen neighbors around the alkane methyl groups (see Figure 14) demonstrates that alkanes preferentially partition into the nonpolar regions of the dry and wet 1-octanol phases. The ethane methyl-octanol carbon (summed over all eight carbon atoms) NIs in dry and wet octanol are compared in Figure 15, and the difference between the two

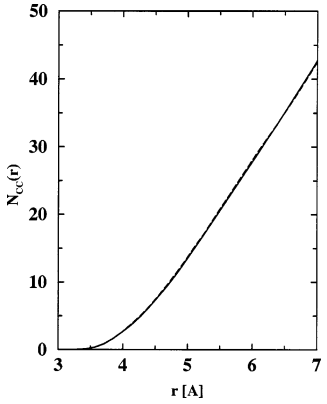

Figure 15. Ethane methyl−octanol carbon (summed over all eight carbon atoms) number integrals in the dry (solid line) and wet (dashed line) octanol phases.

solvent environments is minimal. Since the local solvation environments are indistinguishable for the alkane solutes in dry and wet octanol, it is clear that these solutes avoid the water-rich regions of the wet octanol phase. Thus, the low volume fraction of water in wet 1-octanol results in a reduction of the accessible space for alkane solutes which in turn leads to an increase of the entropic penalty for solvation and the small positive $\Delta G_{O\rightarrow O^*}$ values observed for the alkane solutes (see Table 2).

5. Conclusions

Gibbs ensemble Monte Carlo simulations using the transferable potentials for phase equilibria force field were carried out to investigate the structure of and solute partitioning into neat and water-saturated octanol phases. These simulation demonstrate that water saturation causes a substantial, but nonlocal structural reorganization of the 1-octanol phase which in turn makes wet octanol a more favorable solvent for polar solutes. The great diversity of molecular-scale environments (ranging from the cores of large water-centered micelles over the interfacial regions of these micelles and small 1-octanol aggregates with cyclic or linear architectures to the nonpolar regions created by the alkyl tails) is not reflected in simple structural models proposed earlier (see Figure 1), but it is the likely reason as to why the wet 1-octanol phase can mimic the complexities of many biological or soil environments. In contrast, while aggregates of a wide range of sizes are also found in dry 1-octanol, the local structure of the polar regions presents only one motif, namely a hydroxyl oxygen bound to two neighboring hydroxyls. Finally, the flatness of the distribution over aggregation sizes (see Figure 3) implies that the free energies of these different aggregates are relatively similar. Thus, it appears likely that highly polar or zwitterionic solutes can induce structural changes in their local environment to make it more favorable to them.

Acknowledgment. We thank P. W. Carr, W. G. Miller, and M. H. Abraham for stimulating discussions. Financial support from the National Science Foundations (Grant CHE-0213387) is gratefully acknowledged. Part of the computer resources were provided by the Minnesota Supercomputing Institute.

References and Notes

(1) Sangster, J. *Octanol−Water Partitioning Coefficients: Fundamentals and Physical Chemistry*; John Wiley & Sons: Chichester, U.K., 1997.
(2) Hansch, C.; Leo, A. *QSAR: Fundamentals and Applications in Chemistry and Biology*; American Chemical Society: Washington, DC, 1995.
(3) Hansch, C.; Fujita, T. *J. Am. Chem. Soc.* **1964**, *86*, 1616.
(4) Kamlet, M. J.; Abraham, M. H.; Doherty, R. M.; Taft, R. W. *J. Am. Chem. Soc.* **1984**, *106*, 464.
(5) Connell, D. W. *Bioaccumulation of Xenobiotic Compounds*; CRC Press: Boca Raton, FL, 1990.
(6) Briggs, G. G. *J. Agric. Food Chem.* **1981**, *29*, 1050.
(7) Dobbs, R. A.; Wang, L.; Govind, R. *Environ. Sci. Technol.* **1989**, *23*, 1092.
(8) Marcus, Y. *J. Solution Chem.* **1990**, *19*, 507.
(9) Franks, N. P.; Abraham, M. H.; Lieb, W. R. *J. Pharm. Sci.* **1993**, *82*, 466.
(10) Debolt, S. E.; Kollman, P. A. *J. Am. Chem. Soc.* **1995**, *117*, 5316.
(11) Best, S. A.; Merz, K. M. Reynolds, C. H. *J. Phys. Chem. B* **1999**, *103*, 714.
(12) MacCallum, J. L.; Tielemann, D. P. *J. Am. Chem. Soc.* **2002**, *124*, 15085.
(13) Lawrence, A. S. C.; McDonald, M. P.; Stevens, J. V. *Trans. Faraday Soc*. **1969**, *65*, 3231.
(14) Grunwald, E.; Pan, K.-C.; Effio, A. *J. Phys. Chem.* **1976**, *80*, 2937.
(15) Gestblom, B.; Sjöblom, G. *Acta Chem. Scand.* **1984**, *A38*, 47.
(16) Vahvaselkä, K. S.; Serimaa, R.; Torkkeli, M. *J. Appl. Crystallogr.* **1995**, *28*, 189.
(17) Zachariasen, W. H. *J. Chem. Phys.* **1935**, *3*, 158.
(18) Schantz, M. M.; Matire, D. E. *J. Chromatogr.* **1987**, *391*, 35.
(19) Dallas, A. J.; Carr, P. W. *J. Chem. Soc., Perkin. Trans.* **1992**, *2*, 2155.
(20) Bernazzani, L.; Cabani, S.; Conti, G.; Mollica, V. *J. Chem. Soc., Faraday Trans.* **1995**, *91*, 649.
(21) Chen, B.; Siepmann, J. I. *J. Am. Chem. Soc.* **2000**, *122*, 6464.
(22) Jorgensen, W. L.; Madura, J. D.; Swenson, C. J. *J. Am. Chem. Soc.* **1984**, *106*, 6638.
(23) Jorgensen, W. L. *J. Phys. Chem.* **1986**, *90*, 1276.
(24) Jorgensen, W. L.; Tirado-Rives, J. *J. Am. Chem. Soc.* **1988**, *110*, 1657.
(25) Siepmann, J. I.; Frenkel, D. *Mol. Phys.* **1992**, *75*, 59.
(26) Martin, M. G.; Siepmann, J. I. *J. Phys. Chem.* **1999**, *103*, 4508.
(27) Panagiotopoulos, A. Z.; Quirke, N.; Stapleton, M.; Tildesley, D. *J. Mol. Phys.* **1988**, *63*, 527.
(28) Chen, B.; Siepmann, J. I.; Klein, M. L. *J. Am. Chem. Soc.* **2002**, *124*, 12232.
(29) Wick, C. D.; Siepmann, J. I.; Schure, M. R. *Anal. Chem.* **2002**, *74*, 37.
(30) Wick, C. D.; Siepmann, J. I.; Schure, M. R. *Anal. Chem.* **2004**, *76*, 2886.
(31) Siepmann, J. I.; McDonald, I. R. *Mol. Phys.* **1992**, *75*, 255.
(32) Martin, M. G.; Siepmann, J. I. *J. Am. Chem. Soc.* **1997**, *119*, 8921.
(33) Ben-Naim, A *J. Phys. Chem.* **1978**, *82*, 792.
(34) Martin, M. G.; Siepmann, J. I. *Theo. Chem. Acc.* **1998**, *99*, 347.
(35) Wick, C. D.; Siepmann, J. I.; Schure, M. R. *J. Phys. Chem. B* **2003**, *107*, 10623.
(36) Lyubartsev, A. P.; Martsinovski, A. A.; Shekunov, S. V.; Vorontsov-Velyaminov, P. N. *J. Chem. Phys.* **1991**, *96*, 1776.
(37) Chen, B. Phase Equilibria of Hydrocarbons, Alcohols, Water, and Their Mixtures, Ph.D. dissertation, University of Minnesota, 2001.
(38) Jorgensen, W. L.; Chandrasekhar, J.; Madura, J. D.; Impey, R. W.; Klein, M. L. *J. Chem. Phys.* **1983**, *79*, 926.
(39) Martin, M. G.; Siepmann, J. I. *J. Phys. Chem.* **1998**, *102*, 2569.
(40) Chen, B.; Potoff, J. J.; Siepmann, J. I. *J. Phys. Chem.* **2001**, *105*, 3093.
(41) Allen, M. P.; Tildesley, D. J. *Computer Simulation of Liquids*; Oxford University Press: Oxford, U.K., 1987.
(42) Chen, B,; Siepmann, J. I. *J. Phys. Chem. B* **2000**, *104*, 8725.
(43) Stubbs, J. M.; Siepmann, J. I. *J. Phys. Chem. B* **2002**, *106*, 3968.
(44) Stubbs, J. M.; Siepmann, J. I. *J. Am. Chem. Soc.* **2005**, *127*, 4722.
(45) Wernet, Ph.; Nordlund, D.; Bergmann, U.; Cavalleri, M.; Odelius, M.; Ogasawara, H.; Näslund, L. Å.; Hirsch, T. K.; Ojamäe, L.; Glatzel, P.; Petterson, L. G. M.; Nilsson, A. *Science* **2004**, *304*, 995.
(46) Smith, J. D.; Cappa, C. D.; Wilson, K. R.; Messer, B. M.; Cohen, R. C.; Saykally, R. J. *Science* **2004**, *306*, 851.
(47) McGrath, M. G.; Siepmann, J. I.; Kuo, I.-F. W.; Mundy, C. J.; VandeVondele, J.; Hutter, J.; Mohamed, F.; Krack, M. *J. Phys. Chem. A* **2006**, *110*, 640−646. Published on line September 21, 2005, http://dx.doi.org/10.1021/jp0535949.
(48) Smith, J. D.; Cappa, C. D.; Wilson, K. R.; Cohen, R. C.; Geissler, P. L.; Saykally, R. *J. Proc. Natl. Acad. Sci. U.S.A.* **2005**, *102*, 14171.
(49) To allow for direct comparison with the results of other simulations, a simple distance criterion ($r_{OH} < 2.5$) was used for this part of the analysis.
(50) Dixit, S. P.; Crain, J.; Poon, W. C. K.; Finney, J. L.; Soper, A. K. *Nature* **2002**, *416*, 829.
(51) Ibers, J. A.; Hamilton, W. C. *International Tables for X-ray Crystallography*; Kynoch Press: Birmingham, U.K., 1974.
(52) Cabani, S.; Gianni, P.; Mollica, V.; Lepori, L. *J. Solution Chem.* **1981**, *10*, 563.